SCIENCE CHINA
Chemistry

• ARTICLES •

September 2010 Vol.53 No.9: 2047–2056
doi: 10.1007/s11426-010-4109-6

Size and support effects for CO oxidation on supported Pd catalysts

WANG ZhaoWen, LI Bin, CHEN MingShu*, WENG WeiZheng & WAN HuiLin

State Key Laboratory of Physical Chemistry of Solid Surfaces; National Engineering Laboratory for Green Chemical Productions of Alcohols-Ethers-Esters; Department of Chemistry, College of Chemistry and Chemical Engineering, Xiamen University, Xiamen 361005, China

Received August 2, 2010; accepted August 26, 2010

Supporting Pd catalysts characterized significant different size distribution were obtained using $PdCl_2$, $[Pd(NH_3)_4](NO_3)_2$ and $Pd(acac)_2$ as precursors. High-resolution transmission electron microscopy (TEM), X-ray diffraction (XRD), *in-situ* Fourier transform infrared spectroscopy (FTIR) and Raman spectroscopy were used to examine the dispersion of Pd. Catalytic performance measurements show that the activities for CO oxidation increase as the Pd particle size decreases and the O_2/CO ratio increases. The activities under oxygen rich conditions are significantly higher than those at near the stoichiometric conditions. Pd on TiO_2 prepared by the $Pd(acac)_2$ precursor is highly dispersed, leading to a considerable activity for CO oxidation at near room temperature. CO oxidation on the 1 wt% Pd/TiO_2 and under an O_2/CO ratio of 1 characterized an apparent activation energy of 36.7 kJ/mol, which is closed to those reported for CO oxidation on the supported Au catalysts. The present work demonstrates a high catalytic activity of highly dispersed noble metals, and suggests a promising approach of using noble metals as catalysts with exceeding high efficiency.

noble metals, supported palladium, CO oxidation, size effect, support effect

1 Introduction

The unique properties of palladium and other platinum group metals account for their widespread use. About 25% of goods manufactured today which either contain Pt-group metals or had Pt-group metals play a key role during their manufacturing processes. A large number of catalytic reactions, such as hydrogenation, dehydrogenation, C–C bond formation, as well as in petroleum cracking, are facilitated by Pd-base catalysts. Owing to its outstanding catalytic properties, Pd has been widely used in chemical industry, including in petrochemical, fine chemical, catalytic convertors, water treatment, environmental fields, etc. [1–4]. World demand for palladium increased from 100 tons in 1990 to nearly 300 tons in 2000. The global production of palladium from mines was 222 metric tons in 2006 according to USGS data. Over half of the supply of palladium and its congener platinum goes into catalytic converters in the automobile industry (Platinum group meals, Mineral Commodity Summaries. United States Geological Survey, January 2007). The numerous applications and limited supply sources of palladium have been attracting extensive applied and fundamental researches.

A catalytic convertor cleans the toxic combustion by-products (hydrocarbons, CO, NO_x) from an internal combustion engine by converting to less-toxic substances (H_2O, N_2 and CO_2). The active catalysts in a convertor are the three-way catalysts including Pd, Pt and Rh. Within a narrow fuel/air ratio band surrounding stoichiometry, conversion of all three pollutants is nearly complete. However, outside of that band, conversion efficiency falls off very

*Corresponding author (email: chenms@xmu.edu.cn)

rapidly. When there is more oxygen than required, the system is said to be running lean, and the system is in oxidizing condition. In that case, the converter's two oxidizing reactions (oxidation of CO and hydrocarbons) are favored, at the expense of the reducing reaction. When there is excessive fuel, the engine is running rich. The reduction of NO_x is favored, at the expense of CO and hydrocarbon oxidation. Lean burn refers to the use of a higher air/fuel ratio compared to the stoichiometric combustion ratio of about 14.7. A lean burn mode is a way to improve the combustion efficiency and reduce throttling losses. Thus it is important to understanding the physical chemistry and catalytic properties for the supported Pd catalysts under an oxygen rich condition.

CO oxidation is a typical catalytic reaction [5–24]. Model catalysis and theoretical calculation reveal that CO oxidation on Pt-group metals follows the Langmuir-Hinshelwood (L-H) reaction mechanism [5–12, 16, 18–20]. Goodman *et al.* [9, 16, 18, 20] using polarization-modulation infrared reflection adsorption spectroscopy (PM-IRAS) found that the L-H mechanism fits well with CO oxidation on Pd, Pt and Rh at low pressure (10^{-8}–10^{-3} Torr) to high pressure (1–100 Torr). Chemisorbed oxygen rich surface was found to be more active than a surface palladium oxide and bulk oxide. Previously, we had found that CO oxidation over Pt-group single crystalline surfaces, including Pd, Rh and Pt, exhibits a hyperactive state under oxygen rich conditions with a rate of at least 2–3 orders higher than those at the stoichiometric reaction condition [16, 19, 20].

Regarding the very limited supply of Pd in nature while the high demand, it is very important to improve the dispersion of Pd, as well as other noble metals, on an oxide support surface. In this study, we used various Pd precursors to prepare highly active supported Pd catalysts and characterized their activities for CO oxidation at various reaction conditions.

2 Experiment

2.1 Catalyst preparation

Commercial high-surface area SiO_2 and TiO_2 were used as supports. Mixed-oxide supports of FeO_x/TiO_2 and CeO_x/TiO_2 were prepared by immersing TiO_2 into a certain amount of $Fe(NO_3)_3{\cdot}9H_2O$ or $Ce(NO_3)_3{\cdot}6H_2O$ ethanol solution by stirring at room temperature for 1 h and further aging of 12 h. Then the mixtures were dried and calcined at 400 °C for 2 h.

Pd was deposited onto the above prepared supports by an impregnation method using $PdCl_2$ and $[Pd(NH_3)_4](NO_3)_2$ water solution, and $Pd(acac)_2$ toluene solution as precursors. The supports were added into the certain amount of the precursor solution by stirring at room temperature for 1 h, then aging for 12 h. The mixtures were dried by warming up, and then conditioned at 373 K for 2 h. Then the obtained precursors were calcined at 573 K for 2 h. Here after, the 1 wt% Pd/SiO_2 samples prepared from $PdCl_2$, $[Pd(NH_3)_4](NO_3)_2$ and palladium acetylacetonate ($Pd(acac)_2$) precursors were referred as (a), (b), (c).

2.2 Catalytic test

The CO oxidation reaction was carried out in a continuous-flow fixed-bed quartz microreactor. Typically, 10 mg of catalyst was used. The catalyst was pretreated in O_2 at 573 K for 30 min, swept by He, and then reduced in H_2 at 573 K for 30 min. Reaction gas of 0.5 vol% CO and required amount of O_2 balanced with He, pre-purified by a liquid N_2 trap, was flowed at an ambient pressure through the catalyst bed at a rate of 100 mL/min. The reaction products were quantitatively analyzed using an on-line gas chromatograph (GC) equipped with a methanation convertor and a flame ionization detector (FID).

2.3 Catalyst characterization

The powder X-ray diffraction (XRD) patterns for the structure determination were measured on a Phillips Panalytical X'pert Pro diffractometer equipped with a graphite monochromator. Cu Kα radiation (40 kV and 30 mA) was used as the X-ray source.

The X-ray photoelectron spectroscopy (XPS) was measured with a PHI Quantum 2000 Scanning ESCA Microprobe equipment (physical electronics) using monochromatic Al Kα radiation ($h\nu = 1486.6$ eV). The background pressure in the analysis chamber was lower than 1×10^{-7} Pa. The X-ray beam diameter was 100 μm, and the pass energy was 58.7 eV for each analysis. The binding energies were referenced to the C 1s hydrocarbon peak at 284.6 eV.

Nitrogen physisorption at 77 K was carried out with a Micromeritics Tristar 3000 surface area and porosimeter analyzer to examine the surface area and the porous property of each sample. The samples were pretreated at 573 K in vacuum for 3 h before N_2 adsorption. The specific surface area was calculated following the BET method. The pore diameter distribution was evaluated by the BJH method according to desorption isotherm branch.

The distribution and Pd particles sizes were characterized using a transmission electron microscope (TEM, FEI Tecnai 300 kV).

In-situ Fourier transmission infrared spectroscopy (FTIR, Bruker Vertex 70V) combined with a home-made *in-situ* IR cell, and *in-situ* Raman spectroscopy (Renishaw UV-1000x) combined with a home-made Raman reaction cell. The samples were pretreated by oxidizing in O_2 and reduced in H_2 at 573 K for 30 min.

3 Results and discussion

3.1 Dispersion and particle sizes

Figure 1 shows TEM images of the prepared supported Pd catalysts. The 1 wt% Pd/SiO_2 samples prepared by different precursors, $PdCl_2$, $[Pd(NH_3)_4](NO_3)_2$ and $Pd(acac)_2$, appear significantly different particle sizes. The particle sizes are 50–70, 8–15 and 4–8 nm for the samples prepared from $PdCl_2$, $[Pd(NH_3)_4](NO_3)_2$ and $Pd(acac)_2$, respectively (Figure 1(a)–(c)). The effects of the precursors on the particle sizes of supported metals were proposed to relate with the dispersion, morphology and decomposition of the precursors [24]. Since the $Pd(acac)_2$ precursor leads to the best dispersion of Pd on SiO_2, Pd/TiO_2 was prepared from the $Pd(acac)_2$ precursor. The obtained Pd/TiO_2 sample is absent of Pd particles as shown in the TEM images (Figure 1 (d) and (e)), which suggests Pd is highly dispersed on the TiO_2 support, probably formation of single Pd atoms or two-dimensional (2-D) Pd clusters on the surface. The high dispersion of Pd on TiO_2 is consistent with XRD results which will be shown later. Recent reports also showed highly dispersion of metals on an oxide surface, like Pt on Al_2O_3, in which single Pt atoms on the oxide surfaces are probed by HR-TEM [25, 26].

Figure 2 shows XRD results for the 1 wt% Pd/SiO_2 and Pd/TiO_2 catalysts prepared from the $Pd(acac)_2$ precursor. The XRD spectra are taken after the sample being reduced at 573 K in H_2. Note that the support TiO_2 shows a set of XRD 2θ peaks at 25.4°, 36.9°, 37.8°, 38.5°, 48.1°, 53.9°, 55.1°, 62.7°, 68.6°, 70.4°, 75.1°, corresponding to the crystalline anatase. Note also that the most intense peaks for the metallic palladium and PdO appear at 34.1° and 40.4° respectively. The Pd/SiO_2 sample prepared from $Pd(acac)_2$, particle size of 4–8 nm, shows a weak peak at 34.1° for the metallic palladium. While the Pd/TiO_2 sample is absent of any peak corresponding to a metallic or oxidized palladium. Such comparison reveals that Pd on TiO_2 disperses much better than on SiO_2, though prepared from the same $Pd(acac)_2$ precursor. The absence of the XRD peaks related to Pd and lack of apparent particles in the TEM images for the Pd/TiO_2 sample suggests that Pd is highly dispersed on the support surfaces, formation of individual Pd atoms or 2-D small clusters. The better dispersion of Pd on TiO_2 than on SiO_2 may be related to a stronger metal-support interaction between Pd and TiO_2.

In-situ FTIR spectra for CO adsorption on Pd/SiO_2 and Pd/TiO_2 were compared in Figure 2(b). The saturated pressures for the two samples are 1.33 kPa (10 Torr) and 2.93 kPa (22 Torr), respectively. The gas phase CO bands were subtracted using a comparable IR spectrum for CO gas only. Two IR bands at 2087 and 1954 cm^{-1}, attributed to the atop and bridged adsorption of CO [3, 27], were observed for

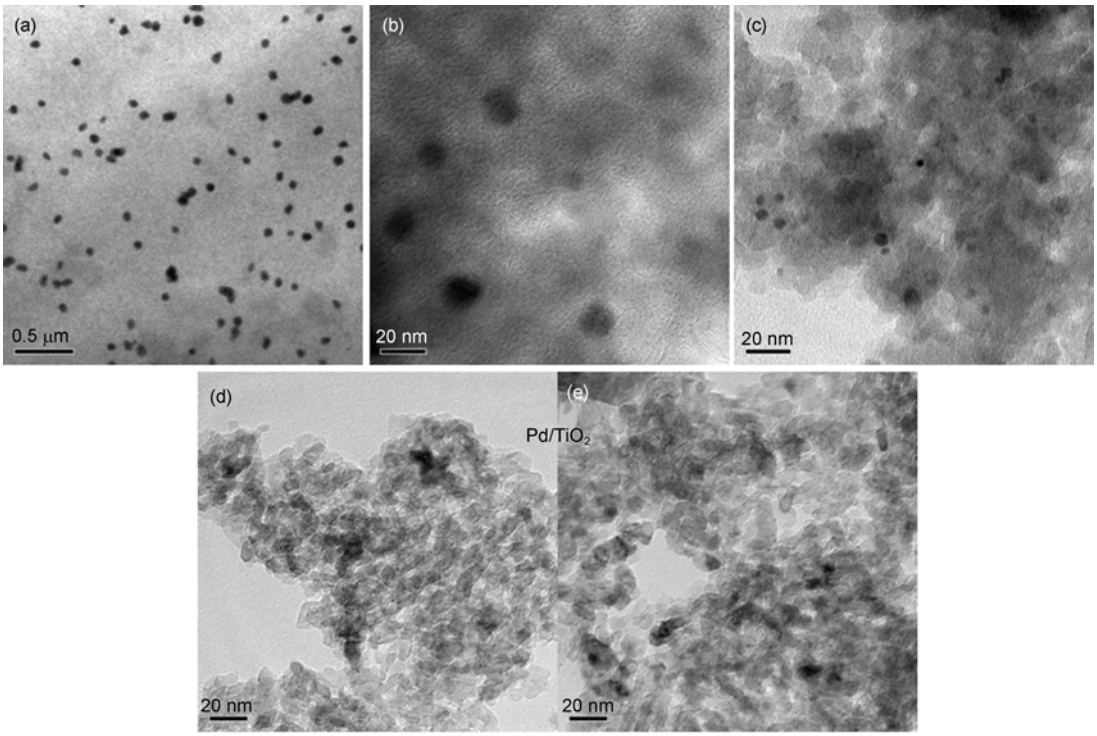

Figure 1 TEM images of the prepared catalysts. (a)–(c) are Pd/SiO_2 prepared from the $PdCl_2$, $[Pd(NH_3)_4](NO_3)_2$ and $Pd(acac)_2$ precursors, respectively. (d) and (e) are Pd/TiO_2 prepared from the $Pd(acac)_2$ precursor.

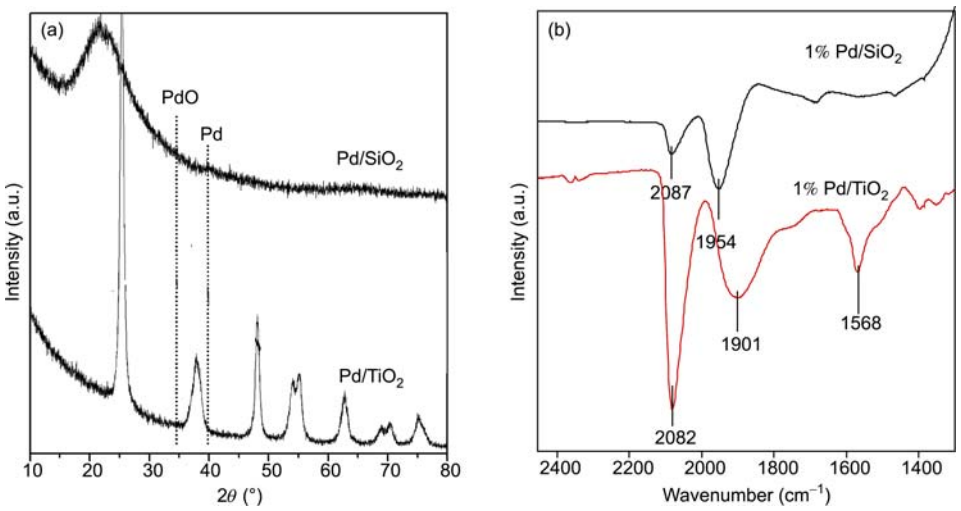

Figure 2 XRD (a) and CO-FTIR spectra (b) for Pd/SiO_2 and Pd/TiO_2 catalysts.

Pd/SiO_2. While 2082 and 1901 cm^{-1} were observed for Pd/TiO_2. The stronger peak for CO atop adsorption on Pd/TiO_2 also confirmed a better dispersion of Pd on TiO_2 than on SiO_2. Moreover, the significant more intense of the atop adsorption feature compared to the bridged adsorption one on Pd/TiO_2 suggests a part of Pd on the surface forms single atoms. Compared to bridged feature of 1954 cm^{-1} for CO on Pd/SiO_2 with a particle size of 4–8 nm, the bridged feature of 1901 cm^{-1} for CO on Pd/TiO_2 may propose a 2-D small clusters on TiO_2, owing to the strong interaction with the support. We would like to emphasize that no band at 2130–2175 cm^{-1} [3, 27] on the both samples, which concludes a metallic Pd on the both supports.

In-situ Raman spectroscopy was used to study the oxidability of different sizes of Pd nanoparticles on SiO_2. Temperature-programmed oxidation of Pd/SiO_2 was shown in Figure 3. In Figure 3(a), Pd particles prepared from $PdCl_2$ with a size of 50–70 nm appear a sharp peak at 648 cm^{-1} above 553 K, which can be assigned to a crystalline PdO [28]. The sample prepared from $[Pd(NH_3)_4](NO_3)_2$ having a particle size of 8–15 nm appears a weak PdO peak when oxidized at 423 K (Figure 3(b)). The Pd/SiO_2 obtained from the $Pd(acac)_2$ precursor appears a very weak PdO peak after oxidized at 423 K. The weak Raman peak is resulted from the poor crystalline of PdO, consistent with small particle size of 4–8 nm (Figure 3(c)). The results demonstrate that smaller Pd particles are much easier to be oxidized than large Pd particles. Which suggests a higher ability to activate a dioxygen molecule under CO oxidation condition, hence possesses a higher catalytic activity for CO oxidation.

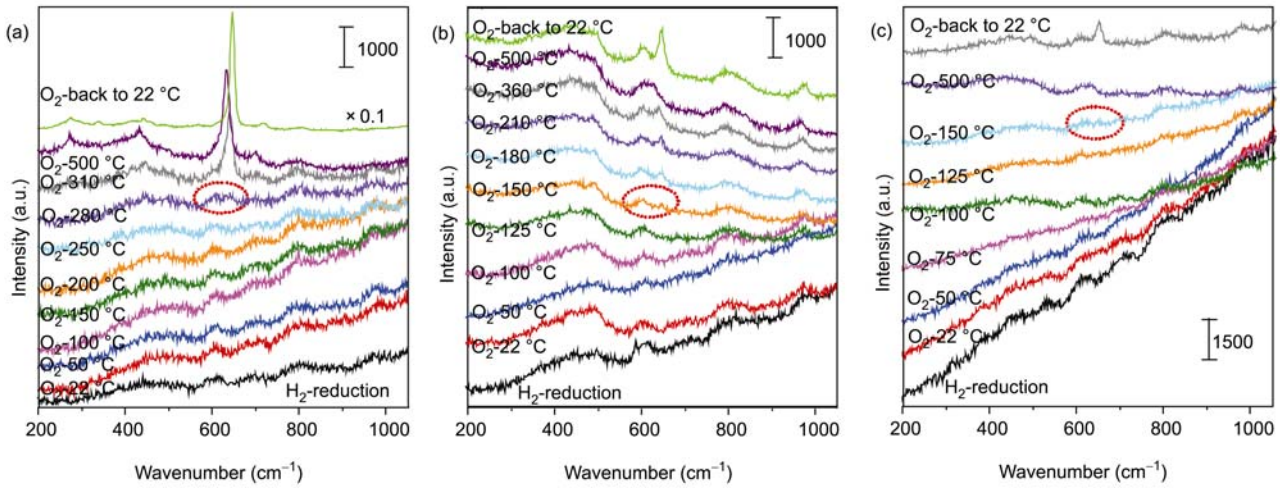

Figure 3 *In situ* Raman spectra for Pd/SiO_2 oxidation at elevated temperature. (a), (b) and (c) correspond to the sample prepared from the $PdCl_2$, $[Pd(NH_3)_4](NO_3)_2$ and $Pd(acac)_2$ precursors, respectively.

3.2 Catalytic performance

Particle sizes and the O_2/CO ratio on the activities for CO oxidation based on the TEM results the particle sizes for the 1 wt% Pd/SiO_2 catalysts prepared from $PdCl_2$, $[Pd(NH_3)_4](NO_3)_2$ and $Pd(acac)_2$ precursors are 50–70, 8–15 and 4–8 nm, respectively. The three samples were noted as (a), (b), (c) in Figure 4. The O_2/CO ratio of 1, 2, 5, 10, 20, 50, 100 examined were marked in Figure 4. The O_2/CO ratio is the molecular ratio, which is equal to P_{O_2}/P_{CO}. The results in Figure 4 show clearly that CO_2 formation rates are enhanced substantially as increase the O_2/CO ratio. The reaction temperature at about 10% CO conversion decreases almost 60 K when the O_2/CO ration increases from 1 to 100. Moreover, the activities were also significantly affected by Pd particle sizes. As the particle size reduced, the activities increase largely. This is more clearly seen by comparing the deferent catalysts at the same reaction condition as shown in Figure 5. Especially, the Pd/TiO_2 catalyst prepared from $Pd(acac)_2$ precursor bears an apparent activity for CO oxidation at room temperature. Here, it is worth to mention that Pd on TiO_2 may form highly dispersive Pd species, like individual Pd atoms and 2-D small cluster, as evidenced by TEM, XRD and FTIR using CO as a probe.

For further evaluating the particle size effect on the catalytic activities, the Pd/TiO_2 sample was sintered by calcining at higher temperatures of 773 and 973 K. As shown in Figure 6(a), the activities drop off significantly as the calcined temperature increases. The XRD characterization for the sintering samples was shown in Figure 6(b) and (c). In both oxidized and reduced samples, the higher temperature calcined leads to appear a XRD feature at 33.5° and 40.5° corresponding to crystalline PdO or Pd, respectively. Which intensities increase as the calcine temperature increases. Whereas, the sample calcined at 573 K doesn't present PdO or Pd XRD peak for the oxidized or reduced palladium, confirmed that Pd is highly dispersive. This set of experiments evidently demonstrated that the low temperature activity for CO oxidation on Pd/TiO_2 is related to the Pd particle size, as well as the support effect.

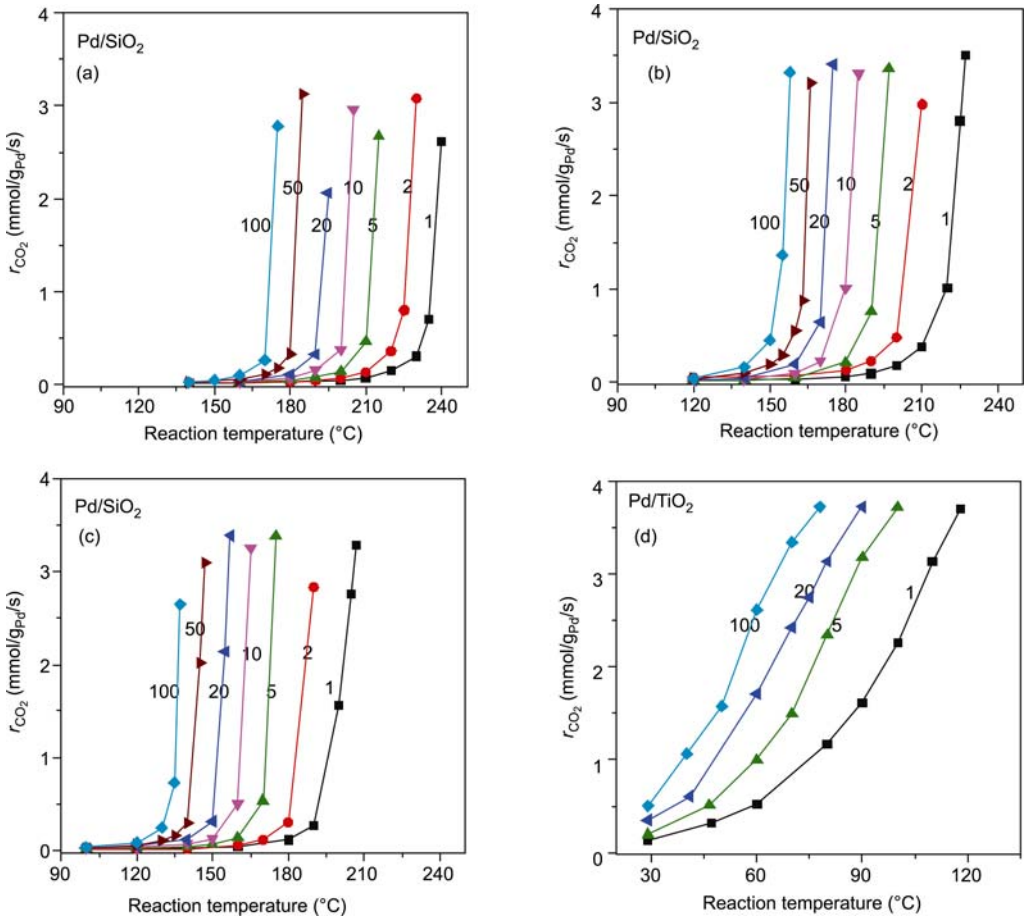

Figure 4 Comparison of CO oxidation on Pd/SiO_2 (a)–(c) and Pd/TiO_2 (d) catalysts. (a)–(c) correspond to the Pd/SiO_2 prepared from $PdCl_2$, $[Pd(NH_3)_4](NO_3)_2$ and $Pd(acac)_2$ precursors, respectively. The O_2/CO ratios are marked for each curve.

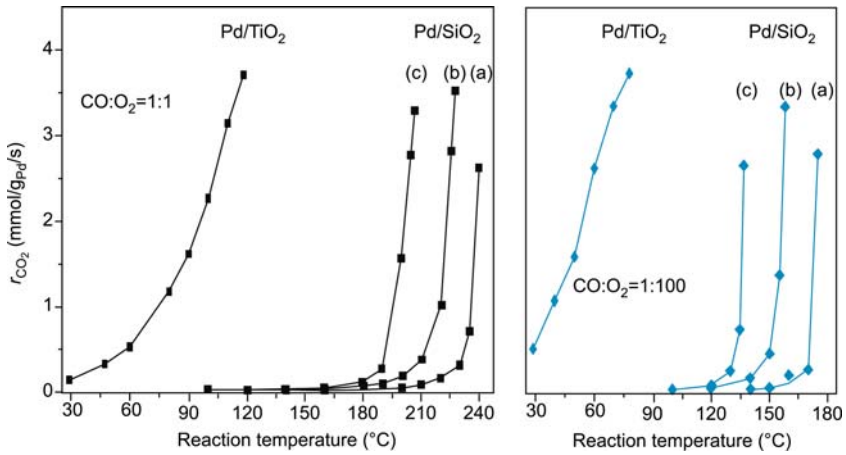

Figure 5 Comparison of CO oxidation on Pd/SiO_2 and the Pd/TiO_2 catalysts O_2/CO ratio of 1 and 100. Line (a)–(c) correspond to the Pd/SiO_2 prepared from $PdCl_2$, $[Pd(NH_3)_4](NO_3)_2$ and $Pd(acac)_2$ precursors, respectively.

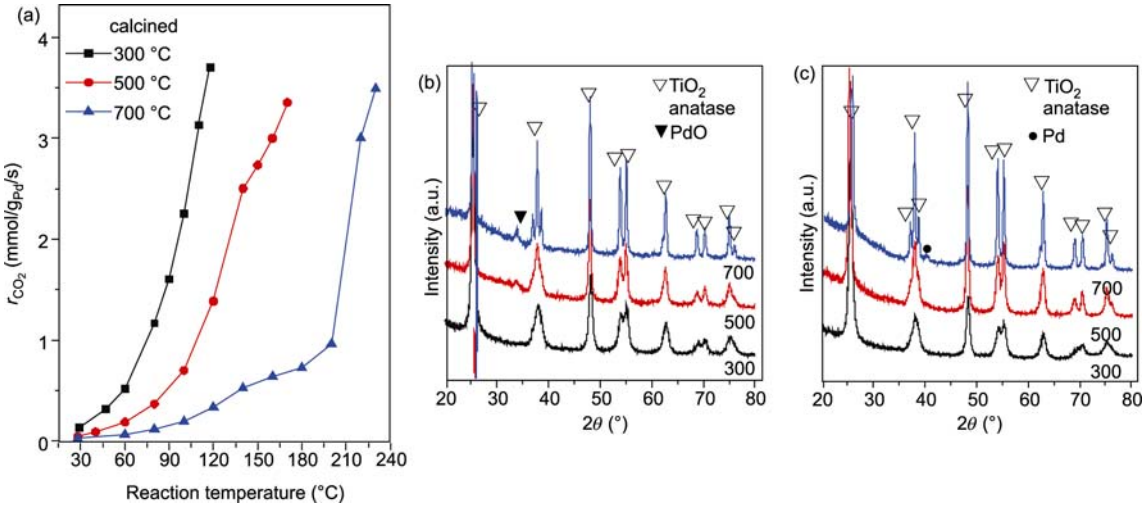

Figure 6 (a) Catalytic activities for CO oxidation on 1 wt% Pd/TiO_2 calcined at different temperatures. XRD spectra for the samples just after being calcined (b) and reduced at 573 K in H_2 (c) .

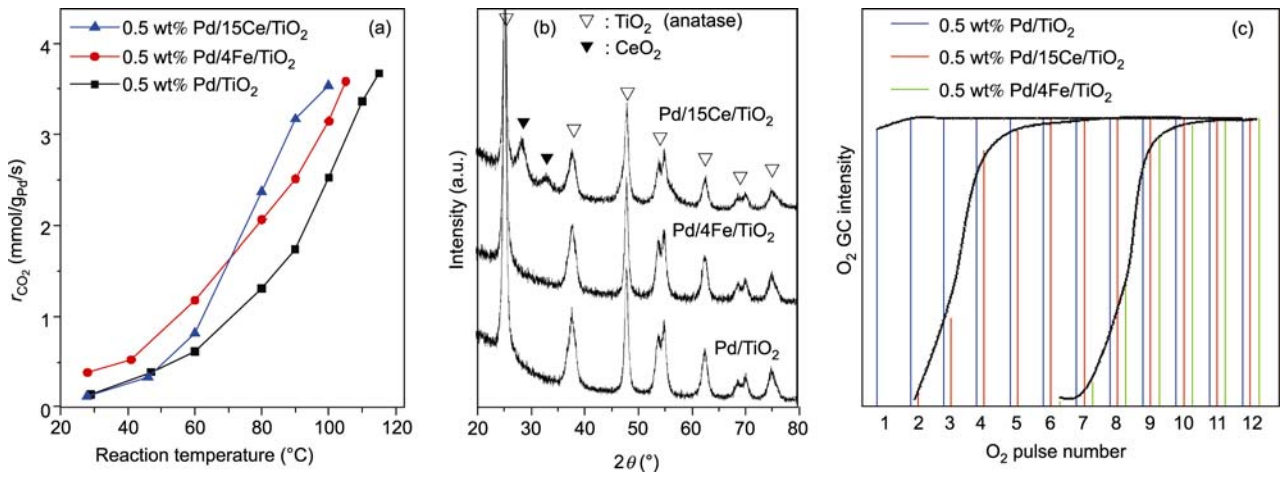

Figure 7 Promotional effects of FeO_x and CeO_2 for CO oxidation on Pd/TiO_2 (a), XRD spectra (b), and oxygen storage amount by an oxygen pulse experiment (c).

Effects of additive: Figure 7(a) shows catalytic activities for CO oxidation on 0.5 wt% Pd/TiO_2 promoted with FeO_x and CeO_x. Here, 0.5 wt% Pd was used instead of 1 wt%, and the total catalyst of 20 mg was used to maintain the same Pd amount. We emphasized that the catalytic activity (per total Pd per second) is proportional to the Pd loading from 0.25 to 2 wt%. This may also support that Pd is highly dispersive on TiO_2 prepared by $Pd(acac)_2$, with all loading Pd having equal activity for CO oxidation, e.g. near 100% dispersion. The promotional effects of FeO_x and CeO_x are apparent in Figure 7(a). It is more efficient at low temperature for FeO_x, while it is at high temperature for CeO_x.

Compared to the unique properties for low temperature CO oxidation on supported Au nanoparticles, the reports for low temperature CO oxidation on supported Pd are very rare. Table 1 listed several literature results for CO oxidation on various supported Pd at near room temperature, as well as our own data. The most reported TOFs (s^{-1}) are about 10^{-3}, except those on Pd/CeO_2 with a TOF of 2.03×10^{-2} at 323 K. We have achieved TOFs of $(2.6-8.7)\times10^{-2}$ over the 1 wt% Pd/TiO_2 and 0.5 wt% Pd/FeO_x/TiO_2 at 313–323 K, which values are significantly higher than the current reported data.

XRD characterization (Figure 7(b)) found crystalline CeO_2 but amorphous FeO_x for 0.5 wt% Pd/CeO_2/TiO_2 and 0.5 wt% Pd/FeO_x/TiO_2, respectively. Pd is highly dispersed without presenting any XRD peak corresponding to PdO or metallic Pd for the 0.5 wt% Pd/TiO_2, 0.5 wt% Pd/4Fe/TiO_2 and 0.5 wt% Pd/15Ce/TiO_2 catalysts.

3.3 Discussion

For CO oxidation over Pt-group metals at near stoichiometric reaction condition, the surface is dominant by CO adsorption. The reaction rate is limited by the adsorption and activation of O_2. And the activation energy is reported to be 92–138 kJ/mol (22–33 kcal/mol), which is closed to the heat of adsorption for CO on Pt-group metals [16]. On model surfaces, we have found that the reaction rates are 2–3 orders higher at an oxygen rich condition than those at near the stoichiometric condition [16, 18–20]. *In situ* IRAS reveals that the surfaces at oxygen rich condition are dominant with chemisorbed oxygen rather than CO at the high rate region.

The above results show that the catalytic activities for CO oxidation over the 1 wt% Pd/SiO_2 and Pd/TiO_2 samples are affected significantly by the Pd particle sizes, O_2/CO ratio and the reaction temperature. Furthermore, the critical temperature (T_C) to achieve the high rate decreases as the particle size decreases, and also decreases as the O_2/CO ratio increases. As shown in Figure 8, the plot of log(O_2/CO) against $1/T_C$ shows a good linear relationship. Surface oxides of transition metals are evidenced to be precursors for their corresponding bulk oxides [31–33]. As proposed by Campbell [31] that the formation of a surface oxide is functions of oxygen pressure and temperature.

For a given reaction,

$$M+\frac{1}{2}O_2 \rightarrow M-O_{ads}$$

Table 1 Comparison of low temperature CO oxidation on supported Pd catalysts

Catalyst	O_2/CO	Reaction Temp. (°C)	TOF (s^{-1}) [a)]	Ref.
Pd/CeO_2	1.2%/2.4% = 0.5	40	4.05×10^{-3}	[1]
		50	2.03×10^{-2}	
Pd/CeO_2(nanorod)	5%/1% = 5	50	2.81×10^{-3}	[27]
Pd/CeO_2-TiO_2	5%/1% = 5	40	4.16×10^{-3}	[29]
		50	7.72×10^{-3}	
$Ce_xPd_{1-x}TiO_6$	20%/2.5% = 8	40	–	[30]
		80	2.32×10^{-2}	
Pd/ZMS-5	25.3%/0.8% = 31.6	40	3.32×10^{-3}	[4]
		50	6.03×10^{-3}	
Pd/TiO_2	0.5%/0.5% = 1	40	2.6×10^{-2}	this work
		50	3.9×10^{-2}	
Pd/FeO_x/TiO_2	0.5%/0.5% = 1	40	6.0×10^{-2}	this work
		50	8.7×10^{-2}	

a) TOF is calculated based on the total Pd loading.

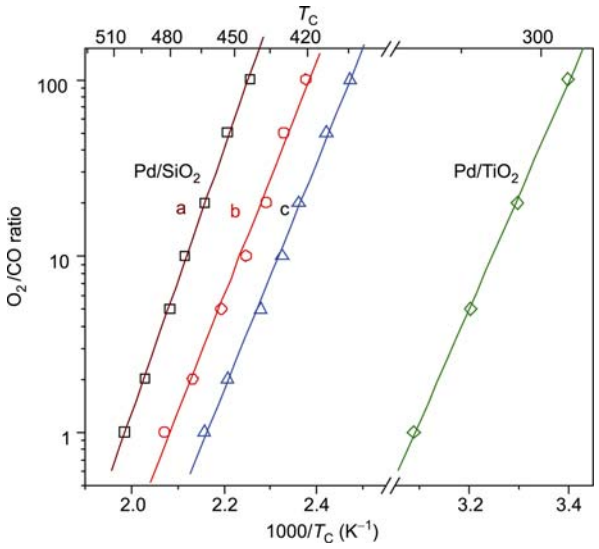

Figure 8 Plots of log(O_2/CO) against 1/T_C. T_C is the temperature to achieve the high rate.

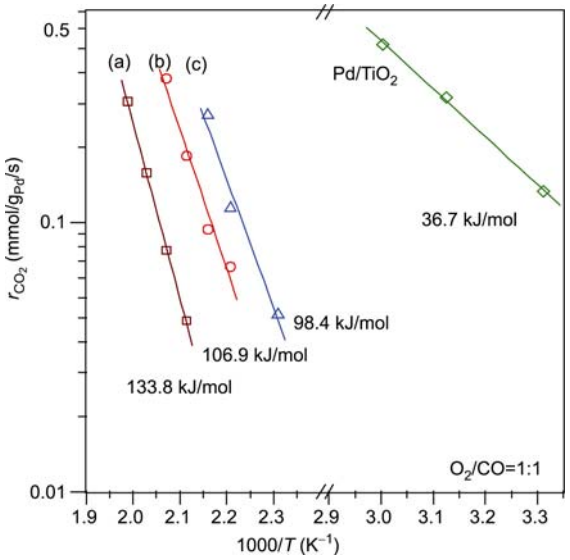

Figure 9 The Arrhenius plots for Pd/SiO_2 and Pd/TiO_2 catalysts.

the kinetic constant can be derived as,

$$K_{eq} = \left(P_{O_2,eq}/P^{\Theta}\right)^{-1/2} = \exp\left(-\Delta G^{\Theta}/RT\right)$$
$$= \exp\left[-\left(\Delta H^{\Theta} - T\Delta S\right)\right]/RT$$

then,

$$\ln\left(P_{O_2,\ eq}/P^{\Theta}\right) = \left(2\Delta H^{\Theta}/R\right)\times(1/T) - 2\Delta S/R$$

which demonstrates a linear relationship of $\ln(P_{O_2,eq})$ against 1/T. Regarding the fact that the active surface transforms from a CO-covered to an O-covered surface at an oxygen rich condition, the surface free energy difference in these two, (G(O)-G(CO)), can be approximated to the heats of adsorption of oxygen and CO, (E_O-E_{CO}). The observation of straight lines in the plots of log(O_2/CO) against 1/T_C provides another experimental evidence supporting the change of the active surfaces from a CO-covered to an O-covered surface. The gradient of each line is slightly different from each other, which may origin from the different binding energies of oxygen and CO on the different sizes of particles [34, 35].

Moreover, the Pd particle size also affects the reaction activation energies. As shown by the Arrhenius plots in Figure 9, the CO_2 formation rate is plotted as a function of 1/T, where the gradients represent the activation energies. Line (a)–(c) correlates with the Pd/SiO_2 catalysts prepared from $PdCl_2$, $[Pd(NH_3)_4](NO_3)_2$ and Pd(acac)$_2$ precursors respectively, which Pd particles are 50–70, 8–15 and 4–8 nm as derived from the TEM images in Figure 1. The activation energies for the three Pd/SiO_2 catalysts are 133.8, 106.9 and 98.4 kJ/mol, respectively, which shows a clear trend of that the activation energy decreases as the particle size decreases. For Pd/TiO_2 catalyst, due to its high dispersion of Pd, the activation energy is only 36.7 kJ/mol, which is closed to those of 7–21 kJ/mol observed for low temperature CO oxidation on supported Au nanoparticles [36–39].

TEM and XRD results both show that Pd on TiO_2 prepared by the Pd(acac)$_2$ precursor is highly dispersed. The significantly higher intensity of CO atop adsorption than that of bridged adsorption on Pd/TiO_2 in FTIR compared to those on Pd/SiO_2 also evidenced a highly dispersed Pd on TiO_2, due to the formation of single Pd atoms and/or small 2-D clusters. Different from CO adsorbed on Pd/SiO_2, CO on Pd/TiO_2 at room temperature also appears weak gas phase CO_2 peaks and surface carbonate species at 1568 and 1351 cm^{-1} [27, 29]. This means CO reacts with the lattice oxygen of the Pd/TiO_2 catalysts, which may be an interface oxygen species between Pd and TiO_2 support, or an inverse spillover oxygen species from the TiO_2 support to Pd. It has been reported that surface OH group may play an important role for low temperature CO oxidation [40, 41]. However, the reaction gas ($CO + O_2 + He$) was further purified by a liquid nitrogen trap in our experiments. The H_2O amount should be negligible. Hence, the OH may not be an active surface species. The highly dispersed Pd species and the active lattice oxygen may be origins of the low temperature activity for CO oxidation on Pd/TiO_2.

Regarding the promotional effects of FeO_x and CeO_2, O_2 adsorption amounts were used to evaluate. Figure 7(c) shows oxygen pulse experiments for 0.5% Pd/TiO_2, 0.5%

Pd/4Fe/TiO_2 and 0.5%Pd/15Ce/TiO_2. Before pulse experiments, the samples was pre-reduced in H_2 at 573 K for one hour. Compared to Pd/TiO_2, oxygen consuming amounts increase apparently, especially on Pd/FeO_x/TiO_2. The oxygen adsorption amounts correlate well with the catalytic activities, in that the higher oxygen consuming amount leads to the higher CO oxidation activity. The promotional effects then may relate with oxygen storage ability of FeO_x, CeO_x, with redox pairs of Fe^{3+}/Fe^{2+} and Ce^{4+}/Ce^{3+}.

4 Conclusion

High reaction rates were observed at an oxygen rich condition for CO oxidation on the Pd/SiO_2 and Pd/TiO_2 catalysts. The catalytic activities increase and the temperatures achieved the high rate decrease as the O_2/CO ratio increases. Significant size effect was observed, in which the smaller the Pd particle size the higher rate achieves. Pd on TiO_2 prepared from a $Pd(acac)_2$ precursor is highly dispersed, resulting of the formation of single Pd atoms and small 2-D clusters, which possesses a high CO oxidation activity at near room temperature. The rates achieved are significantly higher than those reported in literature.

This work was supported by the National Natural Science Foundation of China (20873109), National Basic Research Program of China (973 program) (2005CB221401, 2010CB732303), Major Project of Chinese Ministry of Education (309019), the Ph.D. Programs Foundation of Chinese Ministry of Education (200803841011) and Natural Science Foundation of Fujian Province, China (2008J0168).

1 Bowker M. Automotive catalysis studied by surface science. *Chem Soc Rev*, 2008, 37: 2204–2211
2 Luo MF, Hou ZY, Yuan XX, Zheng XM. Characterization study of CeO_2 supported Pd catalyst for low-temperature carbon monoxide oxidation. *Catal Lett*, 1998, 50: 205–209
3 Zhu HQ, Qin ZF, Shan WJ, Shen WJ, Wang JG. Low-temperature oxidation of CO over Pd/CeO_2-TiO_2 catalysts with different pretreatments. *J Catal*, 2005, 233: 41–50
4 Bi YS, Zhao XH. Catalytic activities for CO oxidation on supported Pd. *Rare Metal Mater Engin*, 2009, 38 (5): 870–875
5 Madey TE, Albert EH, Dietrich M. Adsorption of oxygen and oxidation of CO on the Ru(0001) surface. *Surf Sci*, 1975, 48(2): 304–328
6 Engel T, Ertl G. A molecular beam investigation of the catalytic oxidation of CO on Pd(111). *J Chem Phys*. 1978, 69(3): 1267–1281
7 Campbell CT, Ertl G, Kuipers H, Segner J. A molecular beam study of the catalytic oxidation of CO on a Pt(111) surface. *J Chem Phys*, 1980, 73(11): 5862–5873
8 Lee Ho-ln, White JM. Carbon monoxide oxidation over Ru(001). *J Catal*, 1980, 63: 261–264
9 Peden CHF, Goodman DW, Weisel MD, Hoffmann FM. *In-situ* FT-IRAS study of the CO oxidation reaction over Ru(001): I. Evidence for an Eley-Rideal mechanism at high pressures? *Surf Sci*, 1991, 253: 44–58
10 Liu J, Xu M, Zaera F. Determination of the rate limiting step in the oxidation of CO on Pt(111) surfaces. *Catal Lett*, 1996, 37: 9–13
11 Rainer DR, Koranne M, Vesecky SM, Goodman DW. CO + O_2 and CO + NO reaction over Pd/Al_2O_3 catalysts. *J Phys Chem B*, 1997, 101: 10769–10774
12 Berlowitz PJ, Peden CHF, Goodman DW. Kinetics of CO oxidation on single-crystal Pd, Pt and Ir. *J Phys Chem*, 1998, 92: 5213–5221
13 Stampfl C, Scheffler M. Density-functional theory study of the catalytic oxidation of CO over transition metal surfaces. *Surf Sci*, 1999, 433-435: 119–126
14 Jones IZ, Bennett RA, Bowker M. CO oxidation on Pd(110): A high-resolution XPS and molecular beam study. *Surf Sci*, 1999, 439: 235–248
15 Bowker M, Stone P, Morrall P, Smith R, Bennett R, Perkins N, Kvon R, Pang C, Fourre E, Hall M. Model catalyst studies of the strong metal-support interaction: surface structure identified by STM on Pd nanoparticles on TiO_2(110). *J Catal*, 2005, 234: 172–181
16 Chen MS, Cai Y, Yan Z, Gath KK, Axnanda S, Goodman DW. Highly active surfaces for CO oxidation on Rh, Pd, and Pt. *Surf Sci*, 2007, 601: 5326–5331
17 Sá J, Bernardi J, Anderson JA. Imaging of low temperature induced SMSI on Pd/TiO_2 catalysts. *Catal Lett*, 2007, 114: 91–95
18 McClure SM, Goodman DW. New insights into catalytic CO oxidation on Pt-group metals at elevated pressures. *Chem Phys Lett*, 2009, 469: 1–13
19 Chen MS, Wang XV, Zhang LH, Tang ZY, Wan HL. Active surfaces of the catalytic hyperactivity for CO oxidation on palladium, submitted for publication
20 Gao F, Wang Y, Goodman DW. CO oxidation on Pt-group metals from ultrahigh vacuum to near atmospheric pressures. 2. Palladium and platinum. *J Phys Chem*, 2009, 113(1): 174–181
21 Engel T, Ertl G. Elementary steps in the catalytic oxidation of carbon monoxide on platinum metals. *Adv Catal*, 1979, 28: 1–78
22 Gabasch H, Knop-Gericke A, Schlögl R, Borasio M, Weilach C, Rupprechter G, Penner S, Jenewein B, Hayek K, Klötzer B. Comparison of the reactivity of different Pd-O species in CO oxidation. Phys *Chem Chem Phys*, 2007, 9(4): 533–540
23 Zheng G, Altman EI. The oxidation mechanism of Pd(100). *Surf Sci*, 2002, 504: 253–270
24 Li B, Weng WZ, Wan HL. Unpublished date.
25 Zhang T, Wang AQ, Zheng MY, Ji N, Zhang YH, Huang YQ. Synthesis and catalytic performance of highly dispersed namoparticles. The 27th Chinese Chemical Society, Catalysis Section I-8, Xiamen, 2010
26 Kwak JH, Hu JZ, Mei DH, Yi CW, Kim DH, Peden CHF, Allard LF, Szanyi J. Coordinatively unsaturated Al^{3+} centers as binding sites for active catalyst phases of platinum on gamma-Al_2O_3. *Science*, 2009, 325(5948): 1670–1673
27 Luo JY, Meng M, Yao JS, Li XG, Zha YQ, Wang XT, Zhang TY. One-step synthesis of nanostructured Pd-doped mixed oxides MO_x-CeO_2 (M = Mn, Fe, Co, Ni, Cu) for efficient CO and C_3H_8 total oxidation. *Appl Catal B*, 2009, 87: 92–103
28 McBride JR, Hass KC, Weber WH, Resonance-Raman and lattice-dynamics studies of single-crystal PdO. *Phys Rev B*, 44 (1991) 5016–5028
29 Liang FX, Zhu HQ, Qin ZF, Wang GF, Wang JG. Effects of CO_2 on the stability of Pd/CeO_2-TiO_2 catalyst for low-temperature CO oxidation. *Catal Commun*, 2009, 10: 737–740
30 Wang F, Lu GX. $Ln_xPd_yTi_{1-x-y}O_6$ catalysts: Formation of oxygen vacancy and identification of the active site for CO oxidation. *J Phys Chem C*, 2009, 113: 4161–4167
31 Campbell CT. Transition metal oxides: Extra thermodynamic stability as thin films. *Phys Rev Lett*, 2006, 96: 066106-1
32 Penner S, Bera P, Pedersen S, Ngo LT, Harris JJW, Campbell CT. Interaction of O_2 with Pd nanoparticles on α-Al_2O_3(0001) at low and high O_2 pressures. *J Phys Chem B*, 2006, 110: 24577–24584
33 Zemlyanov D, Aszalo-Kiss B, Kleimenov E, Teschner D, Zafeiratos S, Havecker M, Knop-Gericke A, Schlogl R, Gabasch H, Unterber-

berger W, Hayek, Koltzer B, *In situ* XPS study of Pd(111) oxidation. Part 1: 2D oxidation formation in 10^{-3} mbar O_2. *Surf Sci*, 2006, 600: 983–994

34 Ho YS, Wang CB, Yeh CT. Calorimetric study on interaction of dioxygen with alumina supported palladium. *J Mol Catal A*, 1996, 112: 287–294

35 Wang CB, Yeh CT. Effects of particle size on the progressive oxidation of nanometer platinum by dioxygen. *J Catal*, 1998, 178: 450–456

36 Valden M, Pak S, Lai X, Goodman DW. Structure sensitivity of CO oxidation over model Au/TiO_2 catalysts. *Catal Lett*, 1998, 56: 7–10

37 Berko A, Majzik Z, Kiss AM. Low temperature oxidation on differently prepared TiO_2(110) supported Au catalysts. *J Phys Conf Ser*, 2007, 61: 110–114

38 Chen MS, Goodman DW. Structure-activity relationships in supported Au catalysts. *Catal Today*, 2006, 111: 22–33

39 Chen MS, Goodman DW. Catalytically active gold: From nanoparticles to ultra-thin films. *Acc Chem Res*, 2006, 39: 739–746

40 Fukuoka A, Kimura JI, Oshio T, Sakamoto Y, Ichikawa M. Preferential oxidation of carbon monoxide catalyzed by platinum nanoparticles in mesoporous silica. *J Am Chem Soc*, 2007, 129: 10120–10125

41 Xu LS, Ma YS, Zhang YL, Jiang ZQ, Huang WX, Direct evidence for the interfacial oxidation of CO with hydroxyls catalyzed by Pt/oxide nanocatalysts. *J Am Chem Soc*, 2009, 131: 16366–16367